Influence of Natural Serpentine on the Tribological Performance of Phosphate Bonded Solid Coatings

Zhengchao Xi (xizhengchao@licp.cas.cn)
Lanzhou Institute of Chemical Physics
Jianbo Sun
Aerospace Research Institute of Materials and Processing Technology
Lei Chen
Lanzhou Institute of Chemical Physics
Haixia Cui
Lanzhou Institute of Chemical Physics
Yanjun Ma
Lanzhou Institute of Chemical Physics
Huidi Zhou
Lanzhou Institute of Chemical Physics
Jianmin Chen
Lanzhou Institute of Chemical Physics

Research Article

Keywords: Natural serpentine, Phosphate coating, Anti-wear, Interfacial interaction, Tribo-film

Posted Date: December 13th, 2021

DOI: https://doi.org/10.21203/rs.3.rs-1124090/v1

Version of Record: A version of this preprint was published at Tribology Letters on March 26th, 2022. See the published version at https://doi.org/10.1007/s11249-022-01581-8.

Abstract

Natural serpentine powders were incorporated into phosphate bonded solid coatings to promote the anti-wear performance of the phosphate coatings. Optimal mass percent of natural serpentine in phosphate coatings was firstly explored. Thereafter, in order to stimulate layer slip of natural serpentine and strengthen interfacial interaction between natural serpentine and counterface during the friction process, tribological performance of the composite coatings under different friction condition was properly investigated. The experimental result indicated that the optimal incorporation of natural serpentine in phosphate coatings was 10 wt.%, through which anti-wear performance of phosphate coatings was significantly elevated. Additionally, accompanied by the increase of applied load and sliding speed, natural serpentine was activated by friction force and local friction heat, and simultaneously interfacial interactions between naturals serpentine and counterface were intensified. As a result, a continuous protective tribo-film was in-situ formed on the counterface, through which anti-wear performance of phosphate coatings were significantly promoted. At the same time, serious furrows generated on the counterface were also effectively self-repaired during the friction process, and further abrasion on the counterface was greatly restrained.

1. Introduction

Constant development in the realm of advanced manufacturing, anti-wear performance of the relative machinery parts is urgently waiting to be promoted, and therefore, their maintenance cost could be effectively reduced [1–7]. Phosphate bonded solid coatings possess superior temperature resistance property. But high brittleness and inferior anti-wear performance of the phosphate binder greatly impede its practical application [8–13]. Studies reveled that with appropriate incorporation of functional fillers can effectively promote anti-wear performance of the composite coatings [4–6, 14–24]. Additionally, because process high fracture toughness, fibrous functional fillers can be selected to reduce the brittleness of the composite coatings [11, 25–27].

Natural serpentine, as a kind of layered silicate minerals, is usually applied as lubrication additive and exhibited superb friction-reducing and anti-wear properties in base oil. The possible reasons are mainly attributed to its special micro-structure and excellent physiochemical characteristics. Natural serpentine is mainly composed of magnesium silicate hydroxide [$Mg_3Si_2O_5(OH)_4$], of which silicon oxide tetrahedron and magnesium oxide (hydroxide) octahedron (TO layer) make up the basic unit, and each unit is hold together via Van der Waals forces and hydrogen bonds. Under the friction condition of boundary lubrication and extreme pressure, layer slip of natural serpentine at the friction interface is conducive to promote the friction-reducing performance of the base oil [28–31]. What's more, structural distortion of the MSH at the friction interface also inevitably occurred, through which reactive oxygen functional groups of natural serpentine are released, such as Si-O, Si-O-Si, Mg-O, and Mg-OH. With the stimulation of friction force and local friction heat, these reactive functional groups occurred complex physical and tribo-chemical interactions with tribo-pairs [28, 29, 32–39]. As a result, a protective tribo-film is formed on the surface of tribo-pairs, by which further abrasion on the friction pairs is effectively abated.

According to the special micro-structure and high chemical activity of natural serpentine, it can be selected as the enhanced phase in phosphate bonded solid coatings, and the practical considerations are as follows. On the one hand, the chrysotile (fibrous natural serpentine) contained in natural serpentine possesses higher tensile strength, which is conducive to elevate the toughness of composite coatings. Additionally, reactive hydroxyl of natural serpentine will definitely promote interfacial combination of natural serpentine with phosphate cement during the high-temperature curation process of composite coatings, and therefore, mechanical strength of the composite coating was further promoted. On the other hand, layered micro-structure and high activity of natural serpentine are beneficial to promote friction-reducing and anti-wear properties of phosphate coatings. Specifically, layer slip of natural serpentine at friction interface can reduce the shear force, through which friction-reducing property of phosphate coatings is promoted. Interfacial interaction between natural serpentine and counterface during the friction process can stimulate the formation of tribo-film on the counterface, and anti-wear performance of phosphate coating is accordingly promoted.

Based on the above consideration, in this study, optimal incorporation of natural serpentine powders in phosphate coatings was firstly investigated. And then, in order to stimulate layer slip of natural serpentine and strengthen interfacial interaction between natural serpentine and counterface during the friction process, tribological performance of the composite coatings under different applied loads and sliding speeds was explicitly studied. Finally, the corresponding strengthening mechanism of natural serpentine on tribological performance of phosphate coatings was properly proposed based on the experimental data.

2. Experimental Section

2.1 Materials

Natural serpentine was commercially purchased from Jiangsu Longteng Chemical Co., Ltd (Lianyungang, China). The phosphate cement, mainly composed of chromium magnesium phosphate, was produced by our laboratory, and synthesis process was similar with the reference of [8] and [9]. Deionized water, as the dispersive medium of sprayed paints, was also produced by our laboratory.

2.2 Fabrication of phosphate/natural serpentine composite coatings

Before spraying the composite coatings, the pre-sprayed paint was firstly configured. For the sake of exploring the optimal mass percent of natural serpentine in phosphate coatings, a various of paint systems that contained with 0 wt.%, 5 wt.%, 10 wt.%, 15 wt.%, 20 wt.%, and 25 wt.% natural serpentine were properly prepared, respectively. Additionally, in order to every component was homogenously dispersed in the paint system, the pre-sprayed paint was stirred with superhigh speed blender for at least 5 min. The pre-sprayed substrate (Inconel 718 round block, diameter 24 mm, thickness 7.8 mm) surface was conducted with sand-blasting to a roughness about 1.5 μm (measured by non-contact three-dimensional surface profiler, ISO 25178), which was conducive to the effective combination of substrate with sprayed phosphate coatings. After that, the substrate blocks were cleaned with acetone in a

ultrasonic cleaner for at least 20 min. An artificial spraying gun was employed to spray composite coatings. After the spraying was finished, the wet coatings were placed into a constant temperature drying oven. During the curation process, the temperature in drying oven was firstly rising to 120 ℃ keeping for about 2 h, and then rose to 340 ℃ lasting for about 30 min. The sickness of the composite coatings was about 25±5 μm when measured by the mini gauger (MINITEST 1100 microprocessor coating thickness gauge). The fabricated phosphate/natural serpentine bonded solid coating was noted as PNS composite coating, and when the mass percent of natural serpentine was 10%, the corresponding coating was noted as PNS-10 composite coating.

2.3 Performance characterization

A high-temperature CSM ball-on-disk tribometer (CSM Instrument, Switzerland) was employed to detect the tribological performance of the PNS composite coatings. The commercialized counterpart steel balls (AISI 52100 bearing steel ball, E=210 GPa, HRC 58-63) with a diameter of 6 mm were used as counterface to abrade with the PNS composite coatings. All tribological experiments were conducted under room temperature about 25 ℃ and with a relative humidity about 35%. Friction coefficient of PNS composite coatings was timely recorded by the tribometer. Wear rate (w) of PNS composite coatings was speculated by the formular of $w=V_L/(L\cdot F)$, which represented specific wear volume (V_L) of unit frictional distance (L) and unit applied load (F). Wear volume (V_L) of each PNS composite coating was measured by the non-contact three-dimensional surface profiler (KLA-Tencor MicroXAM-800, America). Each friction experiment was repeated three times in order to reduce error, and the averaged values were finally reported.

2.4 Analytical methods

The morphologies of natural serpentine and composite coatings were observed by field emission scanning electronic microscopy (FESEM, Japan Electronics JSM-6701F). The crystal phase and composition of natural serpentine were detected by high-resolution X-ray diffractometer (HR-XRD, Bruker D8Discover25, Germany). Fourier transform infrared spectrometer (FTIR, Bruker V70, Germany) was used to detect the functional groups of natural serpentine. 3D morphologies as well as contour profiles of wear tracks were observed by non-contact three-dimensional surface profiler (KLA-Tencor MicroXAM-800, America). Surface morphologies and element distribution of the wear spot were tested by field emission scanning electronic microscopy (FESEM, FEI Quanta 650, America) and the affiliated energy dispersive X-ray spectrometer (EDS), separately. X-ray photoelectron spectrometer (XPS, PHI5000, America) was adopted to analyze the chemical bonds contained in wear spot. The specific morphology and composition of the tribo-film section was observed by transmission electron microscopy (TEM, FEI TECNAL G2 S-TWIN F20, America) and spherical aberration corrected transmission electron microscopy (STEM, Titan Cubed Themis G2 300, America).

3. Result And Discussion

3.1 Characterization of natural serpentine and PNS composite coatings

Figure 1(a) and (b) showed XRD spectrum and FTIR spectrum of natural serpentine. The main absorption peaks in XRD spectrum were exactly corresponding to the standard card of PDF#00-002-0094, which depicted the monoclinic magnesium silicate hydroxide $Mg_3Si_2O_5(OH)_4$, and specific crystal face indexes had been properly noted in Figure 1(a). However, there also appeared some weak absorption peaks that belonged to impurities. XRD analysis indicated that the main component contained in the natural serpentine was magnesium silicate hydroxide. FTIR spectrum demonstrated the characteristic functional groups of natural serpentine, and there only appeared absorption peaks of group O-H and group Si-O [40, 41]. The reason why absorption peak of group Mg-O did not appear in the FTIR spectrum was that its wavenumber was located about 450 cm^{-1}, but Figure 1(b) only provided infrared signals that located in wavenumber of 550 cm^{-1} to 4000 cm^{-1}.

The morphologies of the finely grind natural serpentine powders were exhibited in Fig. 2. It was obvious that various morphologies were contained in natural serpentine powders, such as fibrous natural serpentine in Fig. 2(a) and (b), schistose natural serpentine in Fig. 2(c), and granular natural serpentine in Fig. 2(d), respectively. With regard to fibrous natural serpentine, its diameter was about 50 nm, and aspect ratio can achieve two orders of magnitude. Higher tensile strength of fibrous natural serpentine was conducive to reduce the self-brittleness of phosphate coatings. Diameter of the schistose natural serpentine powders reached about 3 μm, at the same time, with small particles and sticks agglomerated onto their surface. Additionally, diameter of small granular natural serpentine was about 50 nm to 800 nm.

The surface morphologies of the fabricated PNS composite coatings were demonstrated in Fig. 3. Mass percent of natural serpentine in Fig. 3(a) and (b) was 0%; mass percent of natural serpentine in Fig. 3(c) and (d) was 10%. Although, the two kind coatings were all appeared different degrees of crack, obvious disparities could still be easily discovered. For coatings without incorporation of natural serpentine, there emerged serious micro cracks and its width can achieve 1 μm to 5 μm. Some cracks were even throughout the total figure and extended to further places of phosphate coating. Along with the water evaporation, volume of the phosphate coatings was rapidly decreased during the curation process, and therefore, micro cracks were inevitably generated on the surface. When it came to the coatings incorporated with 10 wt.% natural serpentine, the situation was significantly improved. Existence of fibrous natural serpentine conspicuously narrowed the width of cracks, and also restrain its further elongation. As a result, the defects of PNS-10 composite coatings were obviously decreased. However, for the reason that the proportion of fibrous natural serpentine was relatively small, some micro cracks still appeared on the surface of PNS-10 composite coatings. More significantly, reactive hydroxyl of natural serpentine would certainly occur interfacial combination with the reactive groups of phosphate cement during high-temperature curation process, by which mechanical strength of the composite coatings can be elevated, and anti-wear performance of the composite coatings can be subsequently promoted.

3.2 Tribological performance of PNS composite coatings

The tribological performance of phosphate composite coatings incorporated with various mass percent of natural se rpentine was demonstrated in Fig. 4, of which the mass percent of natural serpentine increased from 0–25% with an increasing rate of 5%. Fig. 4(a) exhibited the specific friction coefficient and wear rate of each coating, and Fig. 4(b) represented concrete frictional curve of each coating. All experiments were conducted under same friction settings. Specifically, the friction coefficients of PNS composite coatings slightly ascended with the increase of natural serpentine, and when the mass percent of natural serpentine was 20%, the friction coefficient of the composite coatings was in maximum. The same conclusion could also be reflected in Fig. 4(b). However, when it referred to wear rates of PNS composite coatings, its variation trend emerged distinct discrepancy to that of friction coefficients. With the mass percent of natural serpentine increased from 0–25%, wear rate of each coating was firstly decreased and then rapidly increased when content of natural serpentine exceeded 10 wt.%, which illustrated that with incorporation of 10 wt.% natural serpentine, phosphate coatings owned the most excellent anti-wear property, and anti-wear performance was promoted about 55.8%. When mass percent of natural serpentine was less than 10%, the amount of natural serpentine was relatively small, and its strengthening effect was insufficient to phosphate coatings. In contrast, when the mass percent of natural serpentine was more than 10%, the bonding strength between phosphate cement was largely wakened by excessive natural serpentine. Therefore, mechanical strength of the corresponding phosphate coatings was decreased, and as a result, the phosphate coatings with excessive incorporation of natural serpentine behaved deficient anti-wear performance under the same experiment condition. Only when the mass percent of natural serpentine was 10%, anti-wear performance of phosphate coating can be mostly promoted.

The 3D morphologies and contour profiles of wear tracks were exhibited in Fig. 5, of which the mass percent of natural serpentine in Fig. 5(a) and (b) was 0%; in Fig. 5(c) and (d) was 10%; in Fig. 5(e) and (f) was 25%. It was obvious that when phosphate coating was incorporated with 10 wt.% natural serpentine, its wear track in Fig. 5(c) was relatively flat, and abrasion extent was apparently mitigated when compared with that of Fig. 5(a) and (e). This conclusion could also be confirmed by the specific contour line of each wear track. For PNS-10 composite coating, both the width and depth of wear track were simultaneously achieved the minimum value. The experimental results secondly proved that with incorporation of 10 wt.% natural serpentine, anti-wear performance of the phosphate coatings was significantly promoted.

Although anti-wear performance of phosphate coatings was effectively promoted by incorporation of 10 wt.% natural serpentine powders, friction coefficient of PNS-10 composite coatings was still relatively high. Especially, accompanied by the increased mass percent of natural serpentine, friction coefficient of the composite coatings also slightly increased. The possible reason was may attributed to that relatively small friction force under the friction condition of low applied load and sliding speed was insufficient to completely overcome the interlayer force in natural serpentine, which made inferior friction-reducing property of natural serpentine on phosphate coatings. Therefore, performance of PNS-10 composite

coatings under different applied load and sliding speed was investigated, and specific result was shown in Fig. 6. Fig. 6(a) was the tribological performance under different applied load from 2 N to 14 N, in which sliding speed was 8 cm/s, and sliding distance was 150 m. Fig. 6(b) was the tribological performance under different sliding speed from 4 cm/s to 16 cm/s, in which applied load was 11 N, and sliding distance was 150 m. When applied load increased to 8 N, friction coefficient of composite coatings decreased about 21.3%, and when the sliding speed exceeded 8 cm/s, friction coefficient of composite coatings decreased about 15.6%. At the same time, more obvious impact was imposed on the wear rate of composite coatings. Accompanied by the increase of applied load, wear rate was conspicuously declined, which indicated that the anti-wear ability of composite coatings was more significantly promoted when the applied load was increased. In Fig. 6(b), accompanied by the increased sliding speed, wear rate of composite coatings was firstly decreased and then increased. Superhigh sliding speed of 16 cm/s may exceed the speed resistant capacity of the composite coatings and serious abrasion was occurred on the composite coatings, Therefore, increased wear rate was finally exhibited.

Figure 7 exhibited the optical morphologies of wear spots under various friction condition, and the specific experimental settings had been noted on each picture. An obvious variation law could be perceived was that accompanied by the increasing of applied load and sliding speed, rubbing degree appeared on the wear spot was apparently alleviated. And simultaneously, transfer and adhesion of the composite coating on surface of the counterpart steel ball was obviously intensified. What need to be pointed out was that the minimum wear spot area was obtained in Figure 7(f), in which the applied load was 11 N and the sliding speed was 8 cm/s. Such experimental results demonstrated that excellent anti-wear performance of PNS-10 composite coatings under the friction condition of increased applied load and sliding speed in Fig. 6 may related to the adhesion and transfer of composite coatings onto the counterface.

3.3 Strengthening mechanism of natural serpentine on tribological performance of phosphate coatings

For the purpose that explore strengthening mechanism of natural serpentine on tribological performance of phosphate coatings, detailed analyses on the wear spot were conducted. The selected counterpart steel ball was under the friction condition where applied load was 11 N, and sliding speed was 8 cm/s. Elemental analyses on wear spot were demonstrated in Fig. 8, of which Fig. 8(a) was the morphology of the wear spot, Fig. 8(g) was the EDS result of the wear spot, and others was the mapping result of each element on the wear spot. Aside from the counterface element of Fe and C, appearance of element P, O, Mg, Si, and Cr was attributed to the transfer of PNS-10 composite coatings onto the counterface during the friction process. Among them, the mass percent of element O was in maximum, which was because both the phosphate binder and natural serpentine were rich with O. Element P and Cr were from transfer of phosphate cement. Element Mg may come from the transfer of phosphate cement or natural serpentine, and element Si was from the transfer of natural serpentine.

In order to explore the specific role of natural serpentine during the friction process, XPS analysis was conducted on the same wear spot. The concrete results were shown in Fig. 9, of which Fig. 9(a), (b), (c), and (d) was the XPS fine spectrums of Fe2p, P2p, Si2p, and Mg1s, respectively. Chemical bond of Fe-O-Si in Fig. 9(a), indicated that natural serpentine happened isomorphic replacement reaction with the counterface:

$$4Fe + 3O_2 \rightarrow 2Fe_2O_3$$

$$Fe_2O_3 + Mg_3Si_2O_5(OH)_4 \rightarrow Mg_2Fe_2SiO_5(OH)_4 + MgO + SiO_2$$

$$Fe_2O_3 + Mg_3Si_2O_5(OH)_4 \rightarrow Fe_2Si_2O_5(OH)_4 + 3MgO$$

and at the same time, generated the microcrystalline ceramic phase of MgO and SiO_2 on the counterface [28, 32, 35, 36]. Because of the special micro-structure and high chemical activity, natural serpentine possessed high cation exchange capacity. Especially, bigger Mg^{2+} in octahedron layer can be easily replaced by Fe^{3+}, Cr^{3+}, Al^{3+} and etc. What's more, lattice bending and structure distortion of natural serpentine were also inevitably occurred at the friction interface, through which unsaturated chemical bonds such as O-Si-O, Mg-O, and Si-O-Si were released. Under the stimulation of friction force and local friction heat, natural serpentine was prone to generate interfacial interactions with the counterface. Chemical bond of Fe-O-P indicated that phosphate cement also occurred chemical reaction with the counterface. Physical adsorption and tribo-chemical reaction between counterface and natural serpentine as well as phosphate cement greatly intensified adhesion and transfer of composite coating onto the counterface, through which tribo-film can be in-situ formed on the counterface during the friction process [42–48]. What should be noted was that the chemical bond of P-O-M (Metal) in Fig. 9(b) may is P-O-Mg, P-O-Cr, or P-O-Fe. Chemical bonds of Si-O, Si-O-Si, and Mg-O in Fig. 9(c) and (d) may attributed to the transferred natural serpentine, but also may attributed to the newly generated microcrystalline ceramic phase of MgO and SiO_2.

The morphology of tribo-film formed on the counterpart steel ball was shown in Fig. 10. It was clear that a continuous protective tribo-film had generated on the counterface after the friction experiment. At the same time, because of tribo-chemical reaction between counterface and natural serpentine as well as phosphate cement, tribo-film was well combined with the counterface. The thickness of the tribo-film was from 73 nm to 146 nm. The total frictional surface of the counterpart steel ball was completely protected by the generated tribo-film and no exposed area could be observed reflected in Fig. 10(a). However, there were numerous write and black spots contained in the tribo-film exhibited in Fig. 10(b) and (c). For the sake of identifying the concrete chemical composition of these unknowing spots, higher resolution of STEM analysis was conducted. What should be emphasized was that the diffraction contrast between the TEM and STEM was exactly opposite. That was to say, substance with black appearance in TEM images was turned white in STEM images, and vice versa.

Figure 11 was the STEM images of micro particles captured in tribo-film and its composition analyses. Figure 11(a) and (b) exhibited the specific morphology of the particles. Particles in Figure 11(a) was more concentrated and its diameter was only about 3 nm, and diameter of the particle in Figure 11(b) was about 20 nm. Elemental mapping result of Figure 11(b) was reflected in Figure 11(c), which confirmed that the elemental composition of the particle was Ni. Simultaneously, lattice fringe spacing of this particle was also corresponding to the spacing of (111) in cubic Ni. Obviously, because the friction condition was relatively harsh, partial exposure of the substrate was happened during the friction process. Therefore, wear debris of the substrate was embedded in tribo-film. However, for extremely small diameter of particles in Figure 11(a), resolution of the elemental mapping was too poor to identify their elemental composition. But lattice fringe spacing of those particles was exactly corresponding to the spacing of (400) in magnesium silicate hydroxide, which conformed that the particles in Figure 11(a) was super-finely grind natural serpentine powders.

Figure 12 was composition analyses of the black spot reflected in STEM image of tribo-film, which corresponded to the white spot in Fig. 10. Combined with its specific morphology in Figure 12(a) and elemental mapping results of Mg, O, Ni, Cr, and Fe, it could be found that signal strength of each element at the bleak area were apparently reduced. Obviously, elemental composition of the bleak area was not from the phosphate cement, substrate, or counterpart steel ball. Therefore, the only possible result of the bleak area was a hole, which was normal to the formation of tribo-film during the friction process. The reason why mapping result of element Si was not exhibited in Figure 12 was that signals of element Si in STEM analysis was uncharacteristic.

Based on the above analyses of wear spot and tribo-film. The strengthening mechanism of natural serpentine on tribological performance of phosphate coatings can be demonstrated as follows. When applied load and sliding speed were increased, under the stimulation of friction force and local friction heat, natural serpentine was activated and occurred isomorphic replacement reaction with the newly friction-polished counterface, which triggered the formation of tribo-film on the counterface [32, 37, 39]. As the friction process continued, the abrasion and generation of tribo-film finally achieved dynamic equilibrium, and as a result, a certain thickness of tribo-film was in-situ formed on the counterface. Although, numerous micro-holes were inevitably produced during the accumulation process of tribo-film, the captured micro wear debris and super-finely grind natural serpentine powders can effectively fill in these holes, which definitely elevated the compactness of tribo-film. What's more, the newly generated microcrystalline ceramic phase of MgO and SiO_2 not only elevated mechanical strength of the tribo-film, but also definitely promoted anti-wear ability of the tribo-film. Just because existence of such tribo-film at the friction interface, anti-wear performance of the phosphate composite coatings was significantly promoted. At the same time, serious furrows generated on the wear spot during the friction process were also effectively self-repaired by the tribo-film, through which further abrasion on the counterface was greatly restrained.

As for friction-reducing property of phosphate composite coatings, when applied load and sliding speed was increased, layer slip in natural serpentine was boosted, and friction coefficient of the composite

coatings was firstly reduced. But in the later stage of friction experiment, with consumption of natural serpentine as well as accumulation of the hard ceramic phase (MgO and SiO_2) at the friction interface, friction coefficient of the composite coatings was subsequently increased. The conclusion could be proved by the specific friction curves of PNS-10 composite coatings exhibited in Fig. 13, of which Fig. 13(a) was friction curves under increased applied load, and Fig. 13(b) was friction curves under increased sliding speed. As a result, friction-reducing ability of natural serpentine was finite to phosphate composite coatings throughout the total friction process, reflected in Fig. 6.

4. Conclusion

Natural serpentine as the enhanced phase was incorporated into phosphate coatings and its optimal mass percent was 10%, through which anti-wear performance of the phosphate coatings was significantly elevated. Additionally, accompanied by the increase of applied load and sliding speed, anti-wear performance of the composite coatings was further promoted. The possible reason was attributed to that friction force and local friction heat produced by harsh friction condition greatly intensified tribo-chemical reaction between natural serpentine and counterface. As a result, a continuous protective tribo-film was in-situ formed on the counterface, and simultaneously, there also generated the microcrystalline ceramic phase of MgO and SiO_2 on the tribo-film. What's more, numerous micro wear debris and super-finely grind natural serpentine powders were captured in the tribo-film during the friction process. Existence of such tribo-film at the friction interface, anti-wear performance of the phosphate coatings was significantly promoted. At the same time, serious furrows generated on the wear spot during the friction process were also effectively self-repaired by the tribo-film, and further abrasion on the counterface was greatly restrained. However, the friction-reducing ability of natural serpentine to phosphate coatings was finite and friction-reducing performance of the phosphate coatings need further optimization.

Declarations

The authors declare that there are no conflicts of interest involved in this work.

Acknowledgements

Financial assistance of National Natural Science Foundation of China (Grant No.52105228) was greatly appreciated.

References

1. Ye, Y.P., Chen, J.M., Zhou, H.D.: An investigation of friction and wear performances of bonded molybdenum disulfide solid film lubricants in fretting conditions. Wear. **266**, 859–864 (2009)
2. Wan, H.Q., Jia, Y.L., Ye, Y.P.: Tribological behavior of polyimideiepoxy resin-polytetrafluoroethylene bonded solid lubricant coatings filled with in situ-synthesized silver nanoparticles. Progress in

Organic Coatings. **106**, 111–118 (2017)

3. Li, B., Jiang, X.F., Wan, H.Q.: Environment-friendly aqueous PTFE based bonded solid lubricating coatings: Mechanical and tribological properties under diversified environments. Progress in Organic Coatings. **137**, 104904 (2019)
4. Li, B., Jiang, X.F., Wu, Y.P.: Novel environmental-friendly lubricating materials: Water-based PAI-graphite-LaF_3 bonded solid lubricating coatings. Appl. Surf. Sci. **481**, 900–909 (2019)
5. Ma, Y.J., Wan, H.Q., Ye, Y.P.: In-situ synthesis of size-tunable silver sulfide nanoparticles to improve tribological properties of the polytetrafluoroethylene-based nanocomposite lubricating coatings. Tribology International. **148**, 106324 (2020)
6. Jia, Y.L., Wan, H.Q., Chen, L.: Effects of nano-LaF_3 on the friction and wear behaviors of PTFE-based bonded solid lubricating coatings under different lubrication conditions. Appl. Surf. Sci. **382**, 73–79 (2016)
7. Selim, M.S., Shenashen, M.A., El-Safty, S.A.: Recent progress in marine foul-release polymeric nanocomposite coatings. Progress in Materials Science. **87**, 1–32 (2017)
8. Jia, Y.L., Chen, L., Feng, X.Z.: Tribological behavior of molybdenum disulfide bonded solid lubricating coatings cured with organosiloxane-modified phosphate binder. Rsc Advances. **5**, 69606–69615 (2015)
9. Jia, Y.L., Wan, H.Q., Chen, L.: Effects of phosphate binder on the lubricity and wear resistance of graphite coating at elevated temperatures. Surf. Coat. Technol. **315**, 490–497 (2017)
10. Fathyunes, L., Khalil-Allafi, J., Moosavifar, M.: Development of graphene oxide/calcium phosphate coating by pulse electrodeposition on anodized titanium: Biocorrosion and mechanical behavior. Journal of the Mechanical Behavior of Biomedical Materials. **90**, 575–586 (2019)
11. Xu, R.L., Bian, D., Zhao, Y.W.: Tribological behavior studies of chemically bonded phosphate ceramic coatings reinforced with modified multi-walled carbon nanotubes (MWCNTs). International Journal of Applied Ceramic Technology. **17**, 1010–1016 (2020)
12. Khor, K.A., Li, H., Cheang, P.: Processing-microstructure-property relations in HVOF sprayed calcium phosphate based bioceramic coatings. Biomaterials. **24**, 2233–2243 (2003)
13. Qin, Z.B., Xia, D.H., Wu, Z.: Phosphate inorganic coating and its research progress. Surface Technology **48**, 34–42 (2019)
14. Lee, H., Han, G., Kim, M.: High mechanical and tribological stability of an elastic ultrathin overcoating layer for flexible silver nanowire films. Advanced Materials. **27**, 2252–2259 (2015)
15. Gan, C.L., Liang, T., Li, W.: Amine-terminated ionic liquid modified graphene oxide/copper nanocomposite toward efficient lubrication. Appl. Surf. Sci. **491**, 105–115 (2019)
16. Chen, C., Qiu, S.H., Cui, M.J.: Achieving high performance corrosion and wear resistant epoxy coatings via incorporation of noncovalent functionalized graphene. Carbon. **114**, 356–366 (2017)
17. Wu, S.Y., Ladani, R.B., Zhang, J.: Aligning multilayer graphene flakes with an external electric field to improve multifunctional properties of epoxy nanocomposites. Carbon. **94**, 607–618 (2015)

18. Liao, Q.B., Zhang, Q., Wang, X.L.: Facile fabrication of POSS-Modified MoS_2/PMMA nanocomposites with enhanced thermal, mechanical and optical limiting properties. Composites Science and Technology **165**, 388–396 (2018)
19. Song, F.Z., Wang, Q.H., Wang, T.M.: High mechanical and tribological performance of polyimide nanocomposites reinforced by chopped carbon fibers in adverse operating conditions. Composites Science and Technology **134**, 251–257 (2016)
20. Chen, B.B., Li, X., Jia, Y.H.: MoS_2 nanosheets-decorated carbon fiber hybrid for improving the friction and wear properties of polyimide composite. Composites Part a-Applied Science and Manufacturing. **109**, 232–238 (2018)
21. Song, H.J., Zhang, Z.Z., Men, X.H.: Effect of nano-Al_2O_3 surface treatment on the tribological performance of phenolic composite coating. Surf. Coat. Technol. **201**, 3767–3774 (2006)
22. Chen, B.B., Li, X., Jia, Y.H.: Fabrication of ternary hybrid of carbon nanotubes/graphene oxide/MoS_2 and its enhancement on the tribological properties of epoxy composite Chock. Composites Part a-Applied Science and Manufacturing. **115**, 157–165 (2018)
23. Zhao, W.F., Wang, H.Q., Tang, H.T.: Facile preparation of epoxy-based composite with oriented graphite nanosheets. Polymer. **47**, 8401–8405 (2006)
24. Zhang, L., Chen, L., Wan, H.Q.: Synthesis and Tribological Properties of Stearic Acid-Modified Anatase (TiO_2) Nanoparticles. Tribology Letters. **41**, 409–416 (2011)
25. Chawla, K.K., Liu, H., Janczak-Rusch, J.: Microstructure and properties of monazite ($LaPO_4$) coated saphikon fiber/alumina matrix composites. Journal of the European Ceramic Society. **20**, 551–559 (2000)
26. Zhao, X.N., Shi, X.H., Zhang, W.G.: TiAl-nHA composite coatings for sintering protection of carbon fiber and improvement of carbon fiber-hydroxyapatite composites interface. Journal of Alloys and Compounds. **854**, 157027 (2021)
27. Ren, X.L., Turcheniuk, K., Lewis, D.: Iron phosphate coated flexible carbon nanotube fabric as a multifunctional cathode for Na-Ion batteries. Small. **14**, 1703425 (2018)
28. Qi, X.W., Jia, Z.N., Yang, Y.L.: Characterization and auto-restoration mechanism of nanoscale serpentine powder as lubricating oil additive under high temperature. Tribology International. **44**, 805–810 (2011)
29. Zhang, B.S., Xu, Y., Gao, F.: Sliding friction and wear behaviors of surface-coated natural serpentine mineral powders as lubricant additive. Appl. Surf. Sci. **257**, 2540–2549 (2011)
30. Yin, Y.L., Yu, H.L., Wang, H.M.: Friction and wear behaviors of steel/ bronze tribopairs lubricated by oil with serpentine natural mineral additive. Wear. **456-457**, 203387 (2020)
31. Qu, J.J., Qu, H.J., Wen, Z.P.: Self-repairing properties of complex titanium grease containing hydroxyl silicate. Tribology International. **149**, 105685 (2020)
32. Yu, H.L., Xu, Y., Shi, P.J.: Effect of thermal activation on the tribological behaviours of serpentine ultrafine powders as an additive in liquid paraffin. Tribology International. **44**, 1736–1741 (2011)

33. Wang, B.B., Zhong, Z.D., Qiu, H.: Nano serpentine powders as lubricant additive: tribological behaviors and self-repairing performance on worn surface. Nanomaterials. **10**, 992 (2020)
34. Zhang, B.S., Xu, B.S., Xu, Y.: An amorphous Si-O film tribo-induced by natural hydrosilicate powders on ferrous surface. Appl. Surf. Sci. **285**, 759–765 (2013)
35. Chang, Q.Y., Wang, B., Gao, K.: Pressure-dependent anti-wear mechanisms of synthetic magnesium silicate hydroxide nanoparticles. Tribology International. **135**, 230–236 (2019)
36. Qi, X.W., Lu, L., Jia, Z.N.: Comparative tribological properties of magnesium hexasilicate and serpentine powder as lubricating oil additives under High temperature. Tribology International. **49**, 53–57 (2012)
37. Gao, K., Chang, Q.Y., Wang, B.: The tribological performances of modified magnesium silicate hydroxide as lubricant additive. Tribology International. **121**, 64–70 (2018)
38. Yu, Y., Gu, J.L., Kang, F.Y.: Surface restoration induced by lubricant additive of natural minerals. Appl. Surf. Sci. **253**, 7549–7553 (2007)
39. Zhang, B.S., Xu, B.S., Xu, Y.: Cu nanoparticles effect on the tribological properties of hydrosilicate powders as lubricant additive for steel-steel contacts. Tribology International. **44**, 878–886 (2011)
40. Santos, J.C.C., Barboza, A.P.M., Matos, M.J.S.: Exfoliation and characterization of a two-dimensional serpentine-based material. Nanotechnology **30**, 445705 (2019)
41. Yang, Y.L., Ma, J., Qi, X.W.: Fabrication of nano serpentine-potassium acetate intercalation compound and its effect as additive on tribological properties of the fabric self-lubricating liner. Wear. **318**, 202–211 (2014)
42. Li, S.Y., Song, X.S., Kuai, X.X.: A nanoarchitectured $Na_6Fe_5(SO_4)_8$/CNTs cathode for building a low-cost 3.6V sodium-ion full battery with superior sodium storage. Journal of Materials Chemistry A. **7**, 14656–14669 (2019)
43. Shi, J.H., Qiu, F., Yuan, W.B.: Novel electrocatalyst of nanoporous FeP cubes prepared by fast electrodeposition coupling with acid-etching for efficient hydrogen evolution. Electrochimica Acta. **329**, 135185 (2020)
44. Shimizu, M., Tsushima, Y., Arai, S.: Electrochemical Na-insertion/extraction property of Ni-coated black phosphorus prepared by an electroless deposition method. ACS Omega. **2**, 4306–4315 (2017)
45. Yan, G., Feng, X.J., Khan, S.U.: Polyoxometalate and resin-derived P-Doped Mo_2C@N-Doped carbon as a highly efficient hydrogen-evolution reaction catalyst at all pH values. Chemistry-an Asian Journal. **13**, 158–163 (2018)
46. Wu, X.H., Gong, K.L., Zhao, G.Q.: Mechanical synthesis of chemically bonded phosphorus-graphene hybrid as high-temperature lubricating oil additive. Rsc Advances **8**, 4595–4603 (2018)
47. Luo, L., Song, Y., Zhu, C.Z.: Fluorescent silicon nanoparticles-based ratiometric fluorescence immunoassay for sensitive detection of ethyl carbamate in red wine. Sensors and Actuators B-Chemical. **255**, 2742–2749 (2018)

48. Sun, L., Han, C., Wu, N.: High temperature gas sensing performances of silicon carbide nanosheets with an n-p conductivity transition. Rsc Advances. **8**, 13697–13707 (2018)

Figures

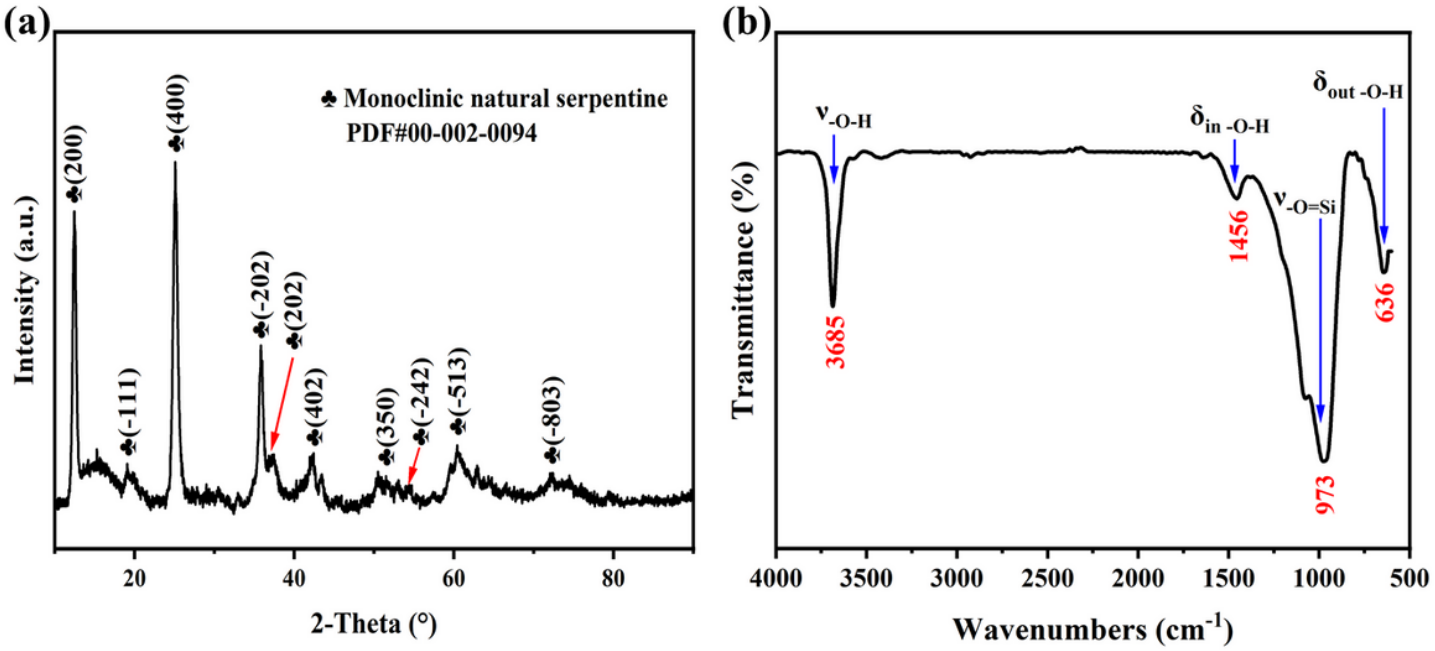

Figure 1

XRD and FTIR spectrums of natural serpentine: (a) XRD spectrum; (b) FTIR spectrum.

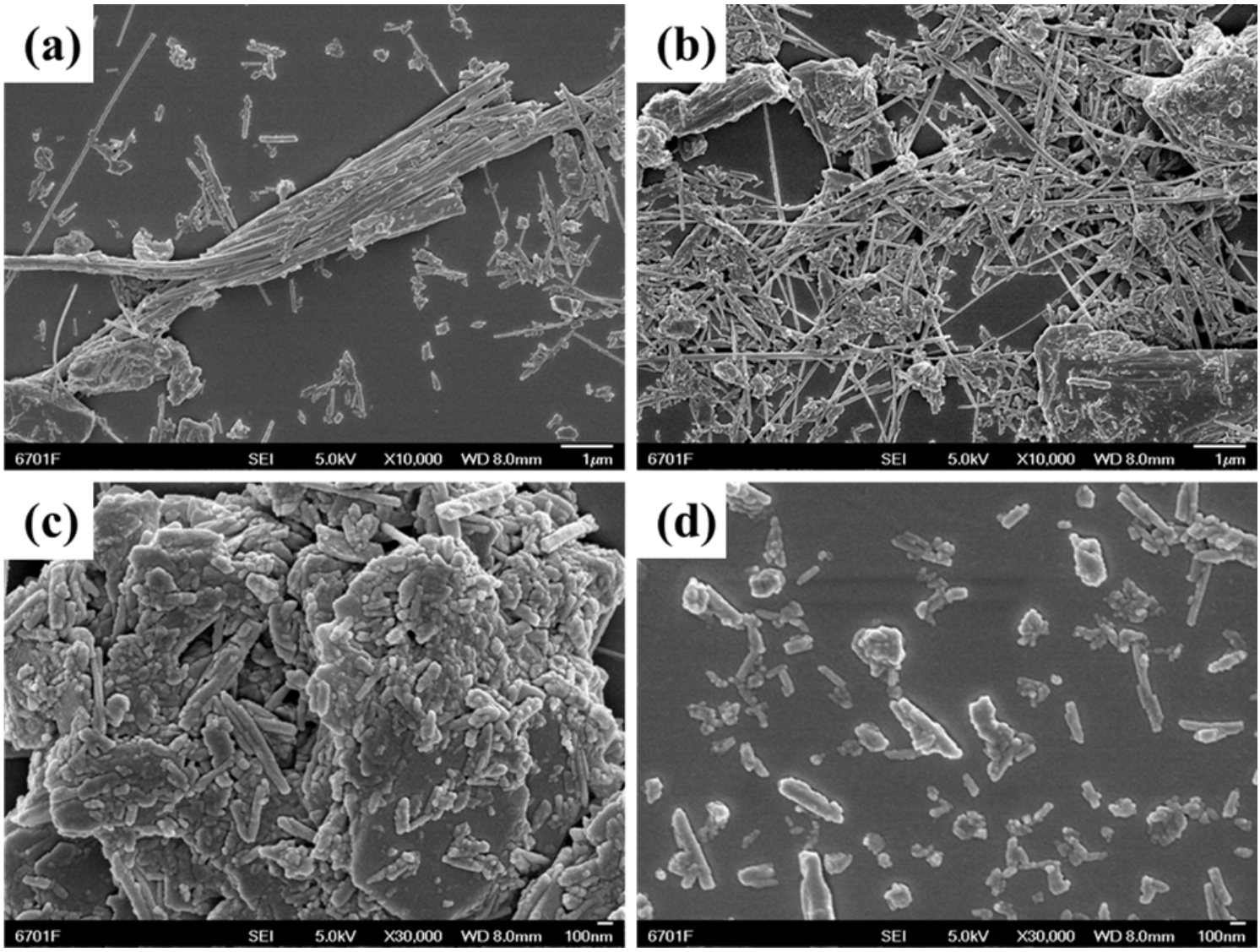

Figure 2

Different morphologies of finely grind natural serpentine powder: (a) and (b) fibrous natural serpentine; (c) schistose natural serpentine; (d) granular natural serpentine.

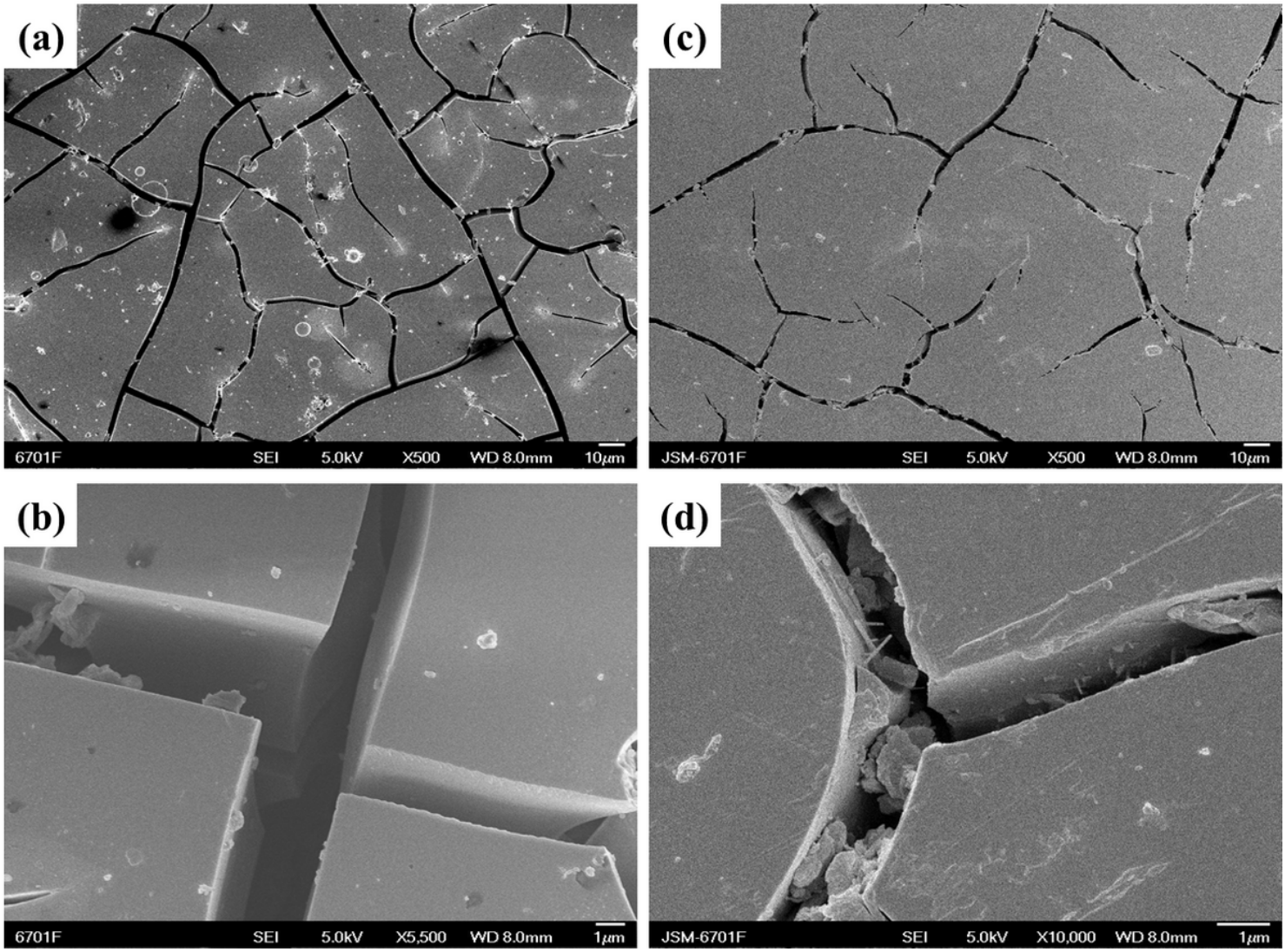

Figure 3

Surface morphologies of PNS composite coatings: (a) and (b) mass percent of natural serpentine was 0%; (c) and (d) mass percent of natural serpentine was 10%.

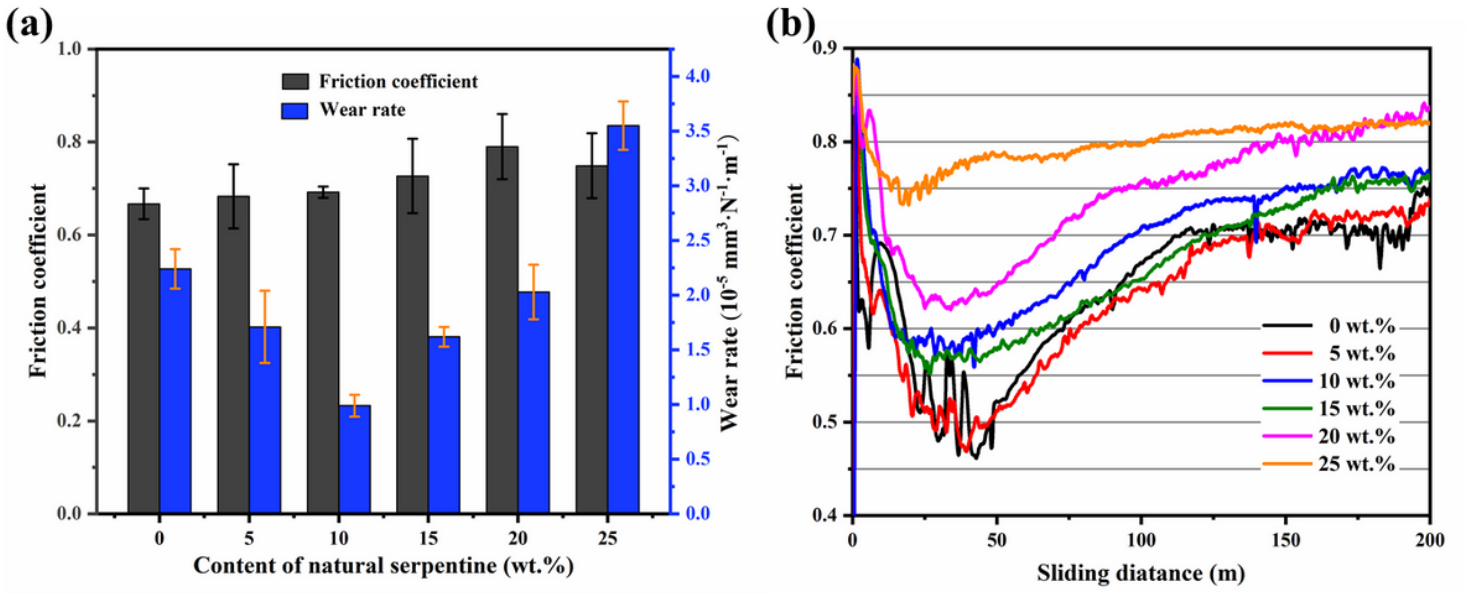

Figure 4

Tribological performance of phosphate composite coatings incorporated with various mass percent of natural serpentine: (a) friction coefficient and wear rate; (b) friction curves. (Applied load 5 N, sliding speed 10 cm/s, sliding distance 200 m)

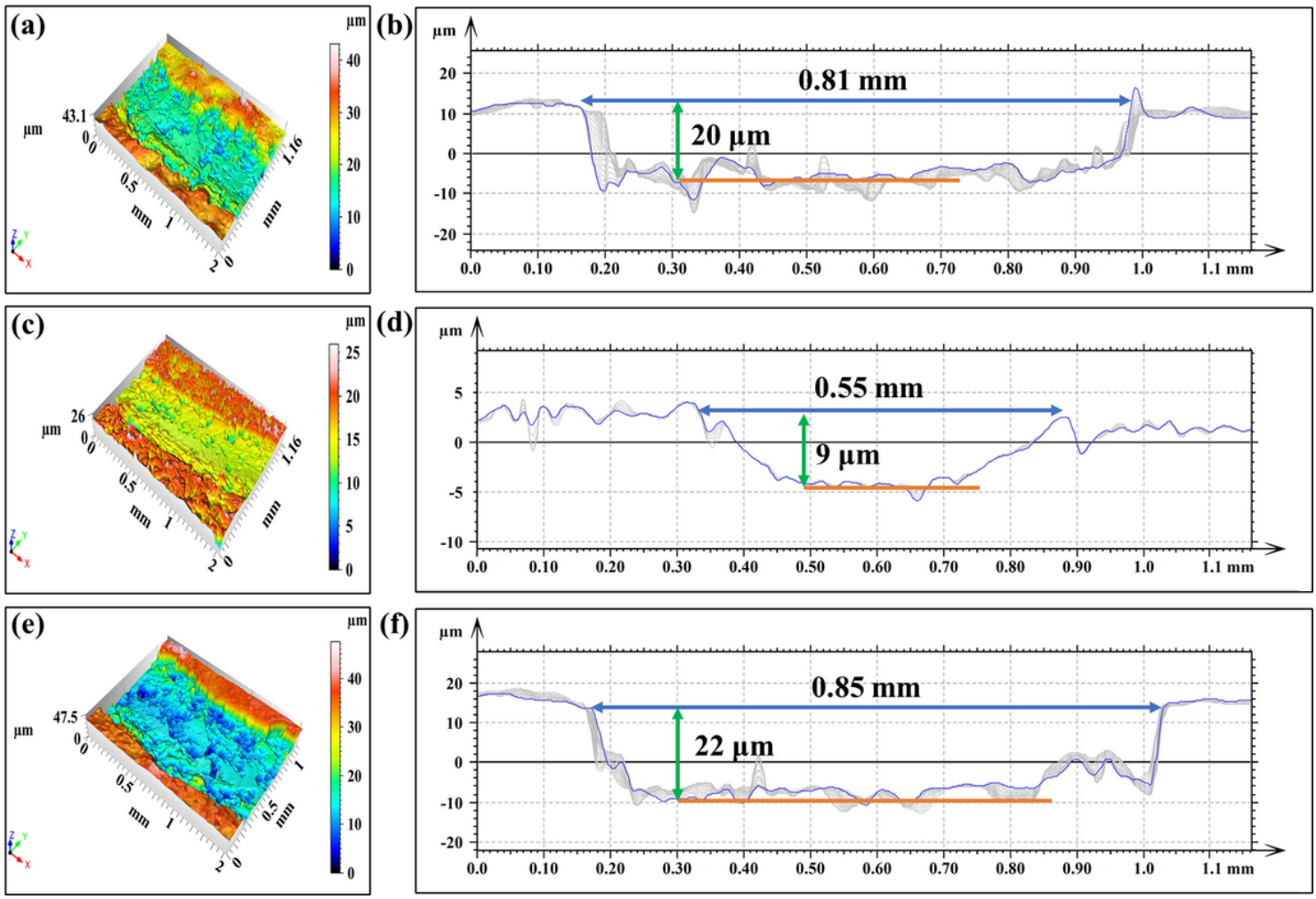

Figure 5

3D morphologies and contour profiles of wear tracks: (a) and (b) mass percent of natural serpentine was 0%; (c) and (d) mass percent of natural serpentine was 10%, (e) and (f) mass percent of natural serpentine was 25%.

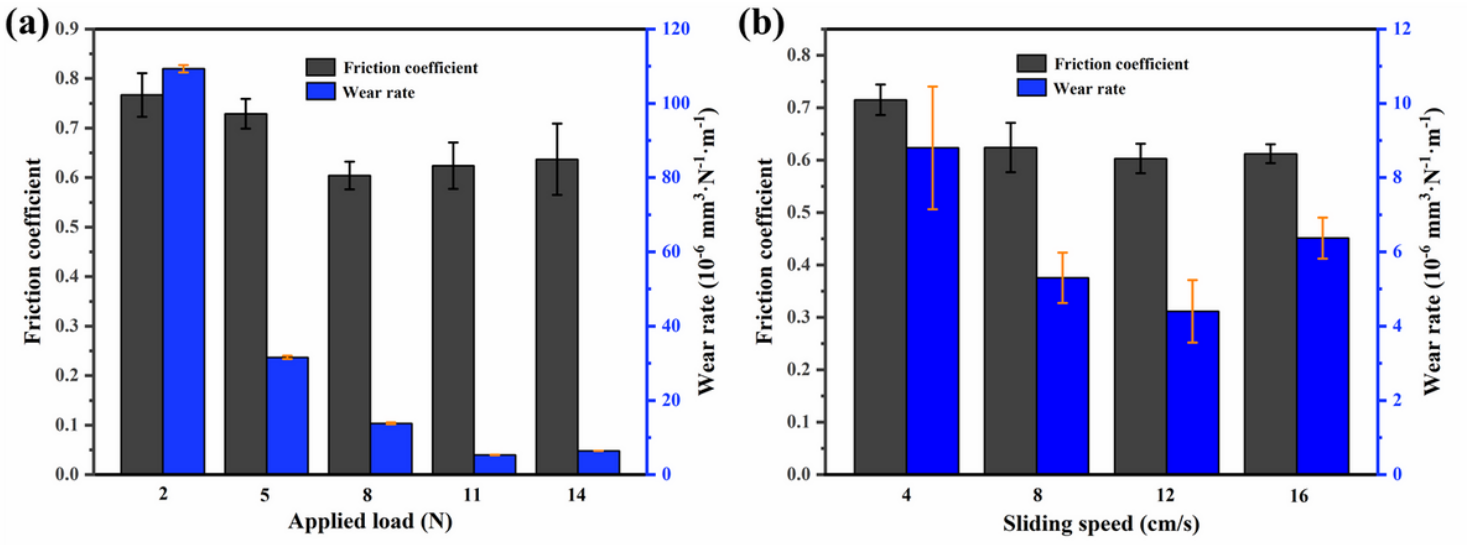

Figure 6

Tribological performance of PNS-10 composite coatings under different applied load and sliding speed: (a) friction coefficient and wear rate under different applied load, (Sliding speed 8 cm/s, sliding distance 150 m); (b) friction coefficient and wear rate under different sliding speed. (Applied load 11 N, sliding distance 150 m)

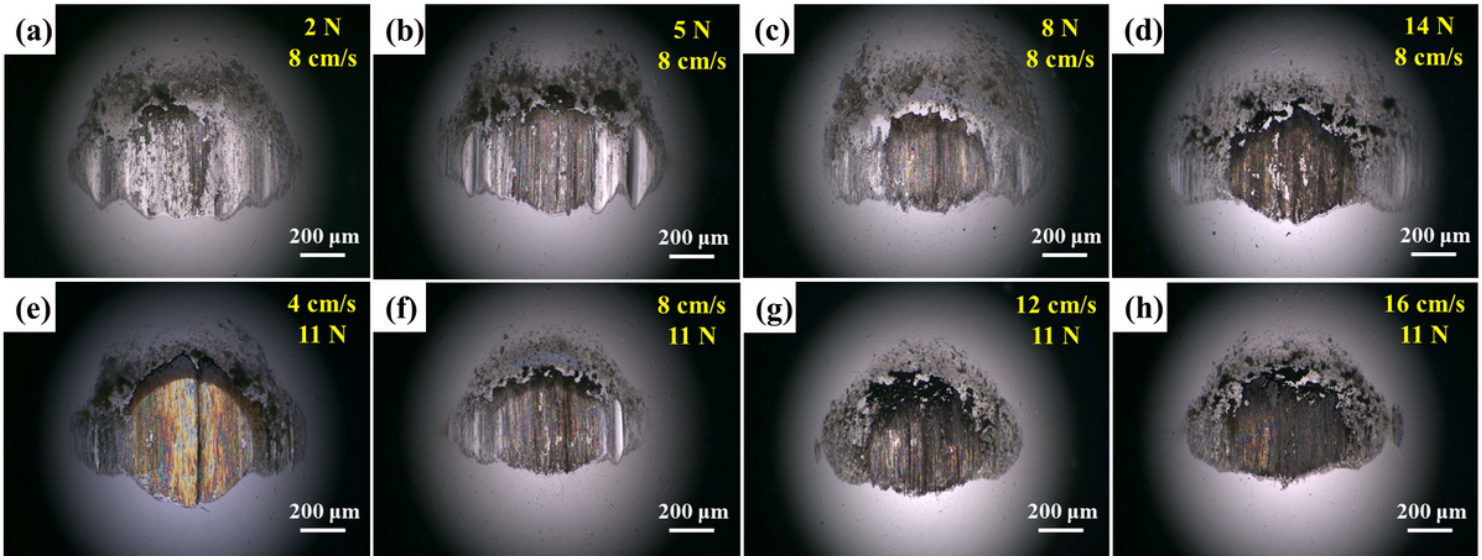

Figure 7

Optical morphologies of wear spots under different applied load and sliding

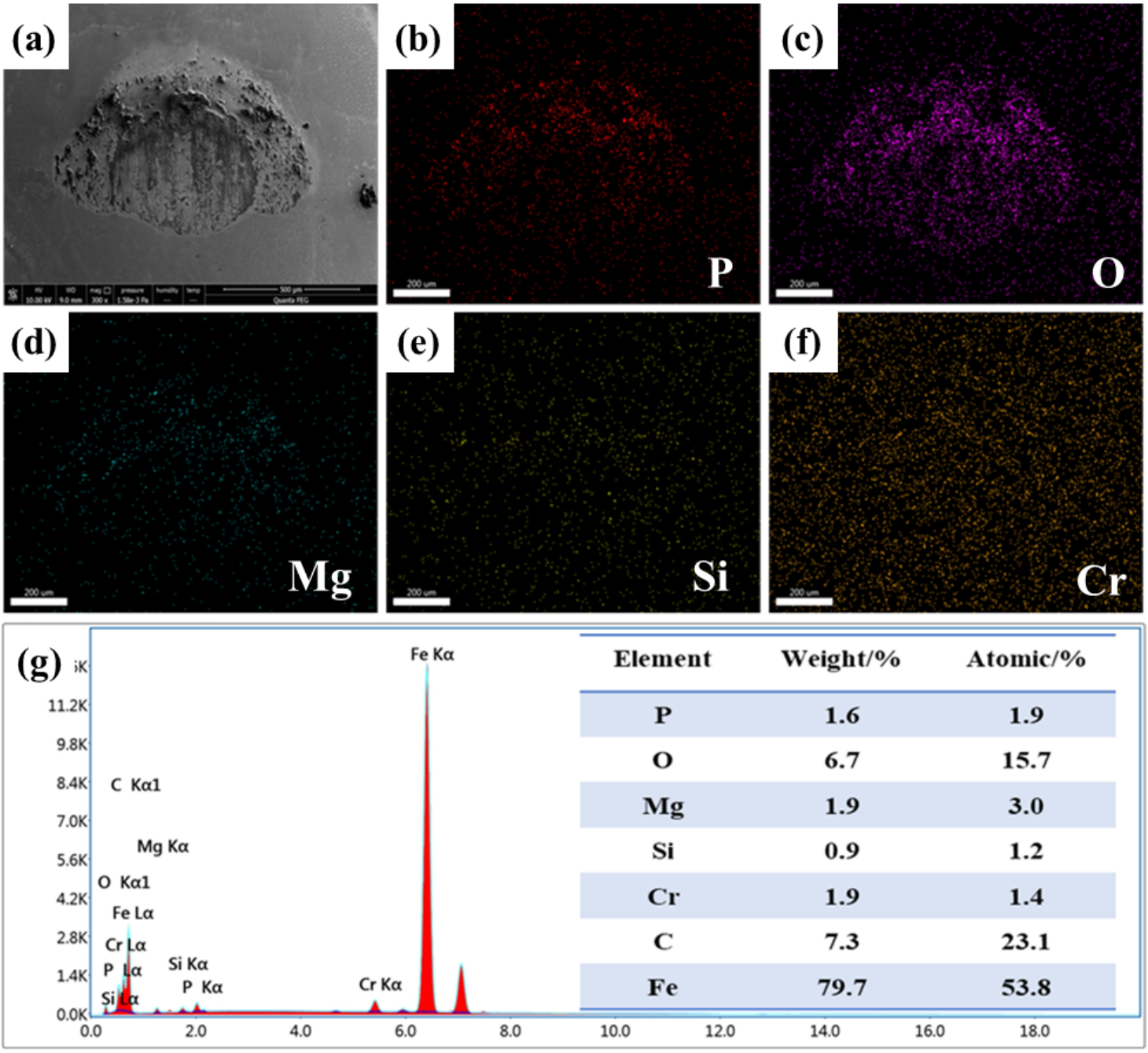

Element	Weight/%	Atomic/%
P	1.6	1.9
O	6.7	15.7
Mg	1.9	3.0
Si	0.9	1.2
Cr	1.9	1.4
C	7.3	23.1
Fe	79.7	53.8

Figure 8

Surface morphology and elemental analyses of wear spot: (a) surface morphology; (b), (c), (d), (e), and (f) elemental mapping result; (g) EDS result.

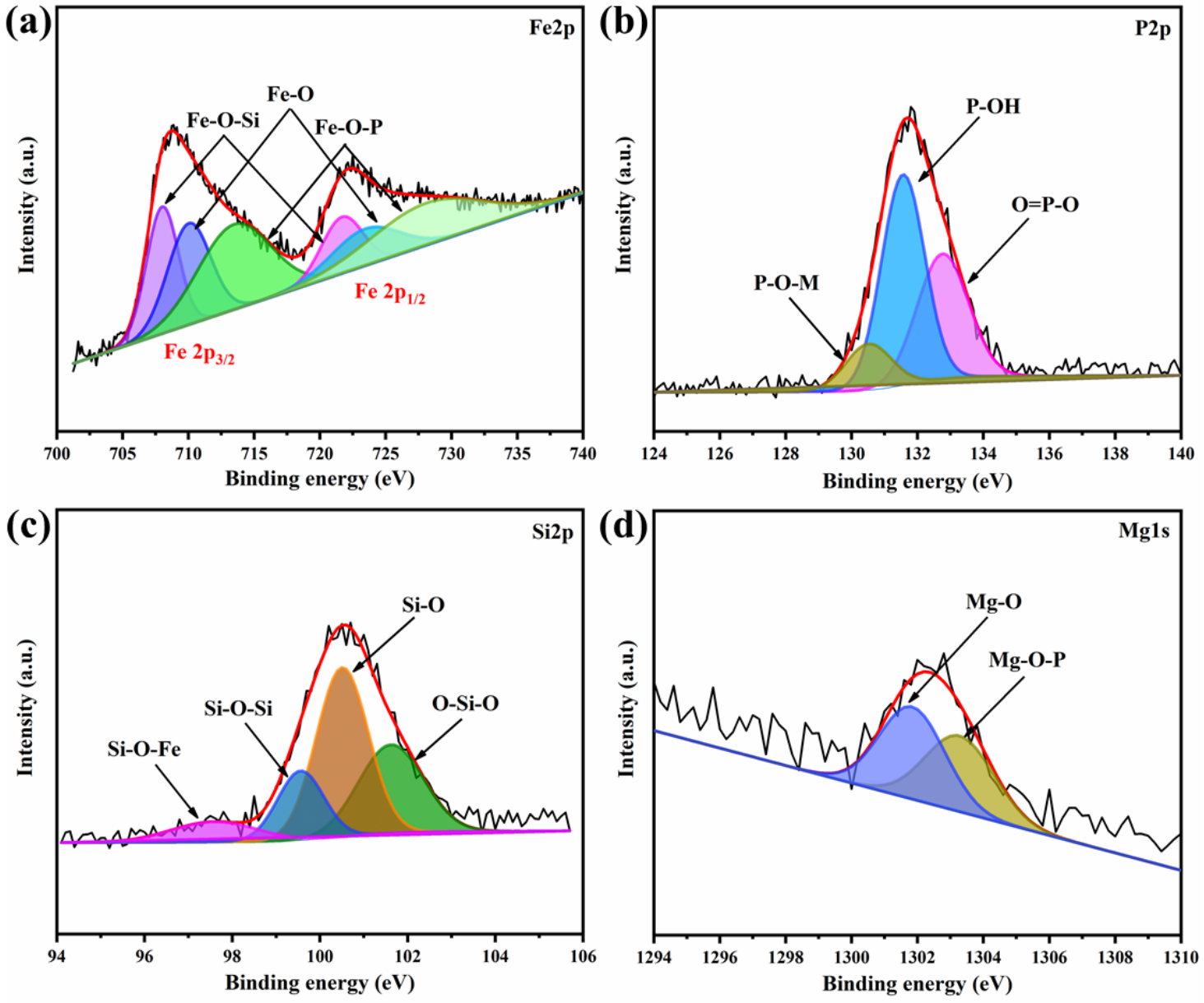

Figure 9

XPS spectrums of wear spot: (a) Fe2p; (b) P2p; (c) Si2p; (d) Mg1s.

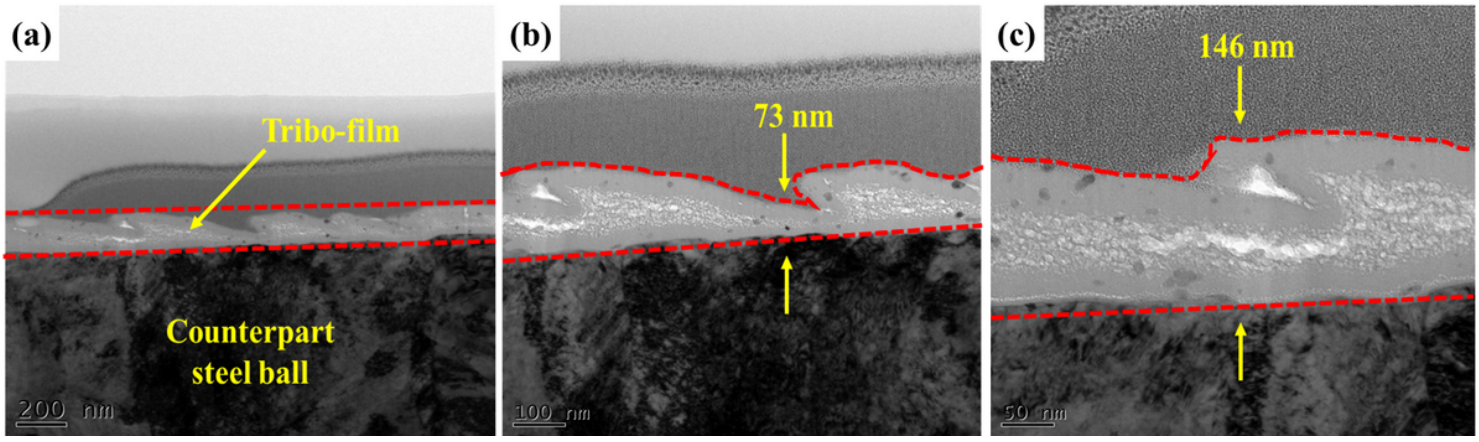

Figure 10

Morphology of tribo-film formed on the surface of counterpart steel ball.

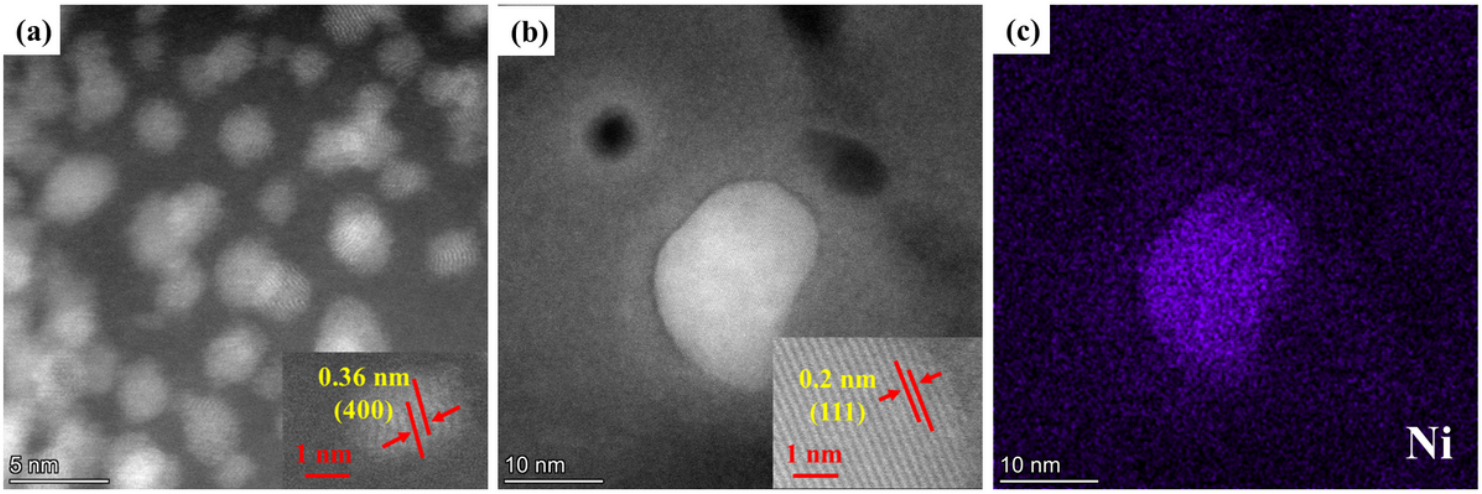

Figure 11

STEM images and composition analyses of particles captured in tribo-film: (a) and (b) morphology of captured particles; (c) elemental mapping result of (b).

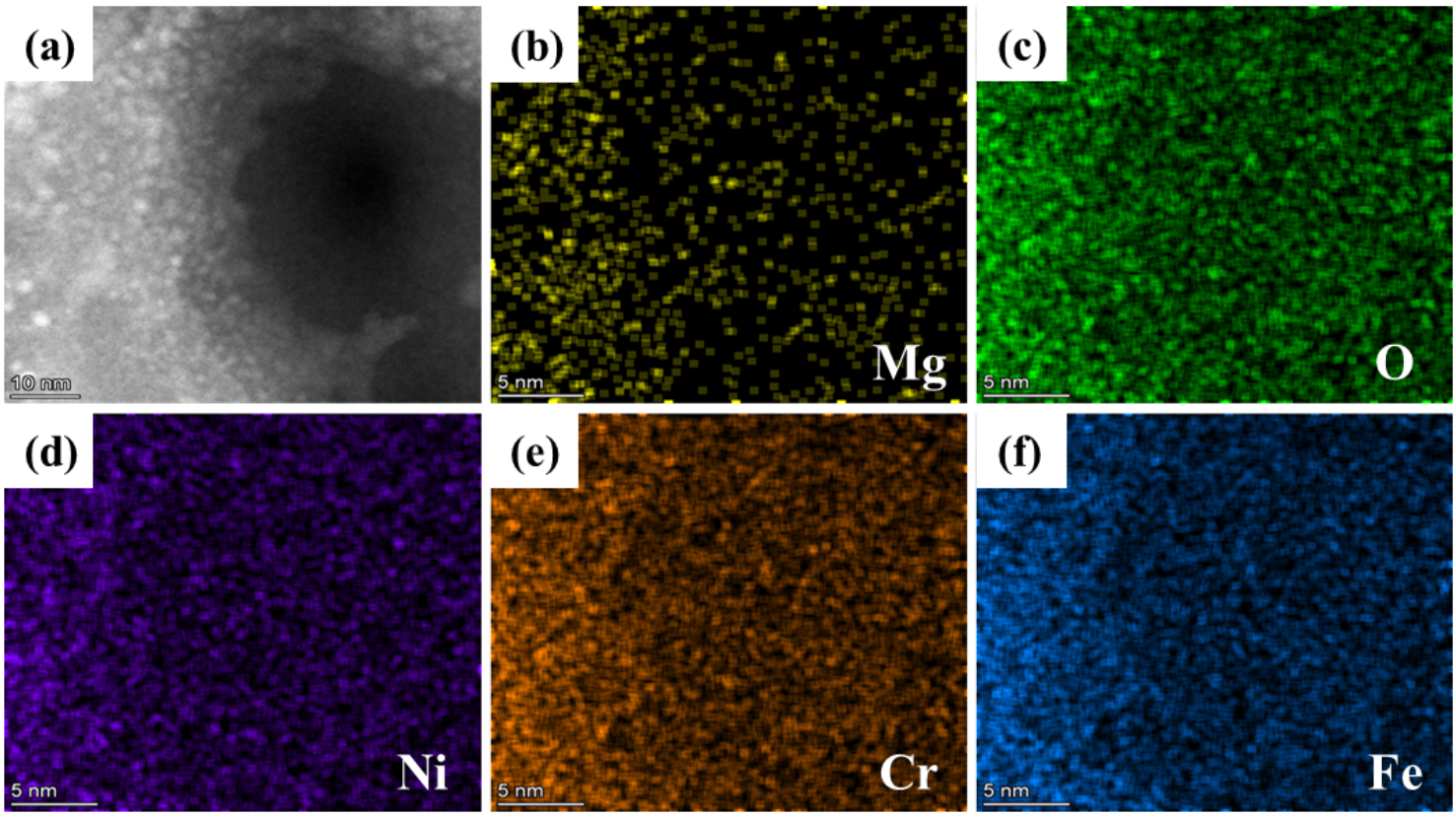

Figure 12

Composition analyses of black spot in STEM image of tribo-film: (a) morphology of black spot; (b), (c), (d), (e), and (f) elemental mapping result.

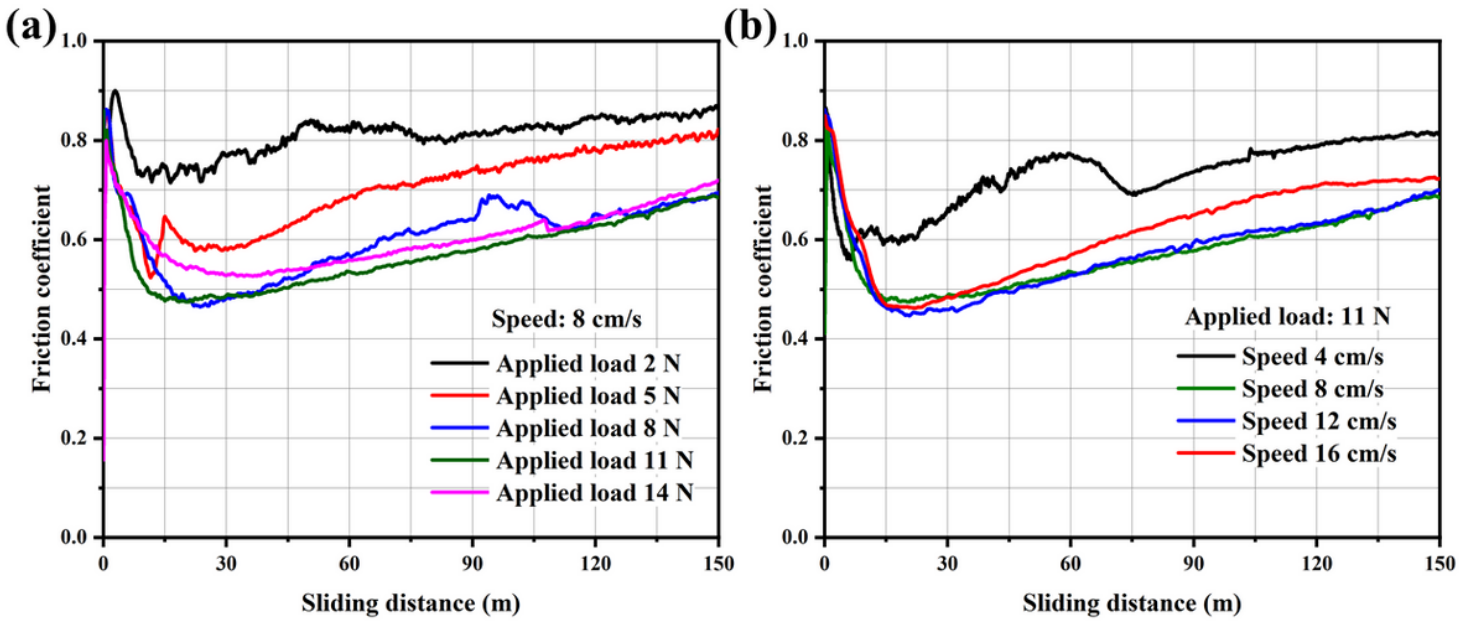

Figure 13

Friction curves of PNS-10 composite coatings under increased applied load and sliding speed: (a) friction curves under increased applied load; (b) friction curves under increased sliding speed.